CHAPTER 4

SPECIFIC AIM 2

4.1 Introduction

The findings in Aim 1 (Chapter 3 on page 22) showed that while using a prosthesis, parietal and motor areas demonstrated an anticipatory effect during reaching when vibrotactile feedback was to be available during the upcoming transport phase of the task. The increased desynchronization in parietal areas, as well as increased synchronization in motor areas, may both serve to build the naïve user's sensorimotor model of the relationships between their motor output and the concomitant sensory feedback (Brickwedde, Krüger, & Dinse, 2019; Sigala et al., 2014; Fell & Axmacher, 2011). Ongoing use of the prosthesis results in updating the sensorimotor model, as well as the model's use as a template to help ensure successful task completion (Sabes, 2000; Wolpert, Doya, & Kawato, 2003). In addition to these functions, the sensorimotor model also serves to help us understand the intentions of people we observe performing motor actions.

The relationships between motor output and its sensory (visual, somatosensory) effects are elements in the lowest-level node of a network of brain areas known as the action observation network (Kilner, Friston, & Frith, 2007; Urgen & Saygin, 2020; Rizzolatti & Craighero, 2004; Saygin, 2007). Figure 1.2 on page 4 shows a schematic diagram of these areas and their interconnections. Information flows from lower-level brain areas that process kinematics into their probable motor commands, a second area transforms those motor commands to the probable goals that would result, and the final area transforms goals into the probable intention of the action. There are reciprocal connections that generate probable intention, goal, and motor information at each step based on the observer's prior experience, context of the environment, and other factors (Kilner, Friston, & Frith, 2007).

Comparisons between the generative information and the processed sensory input result in refinement of the predictions at each step. The end result being a likely intention for the observed person's actions.

The ability to assess the intention of the actions of others based on their movements are key to our ability to understand and interact with others. Prior work from our lab has shown some of the neural effects of observing the actions of others and includes Cusack et al. (2012) which studied the effects of watching a hand or prosthesis when the observer was using a prosthesis. Other work by Mizelle and Wheaton (2010) showed the neural effects of observing correct and incorrect tool use, and work by Natraj et al. (2013) showed the effect of context while using tools. Many other studies have been conducted in which participants using their hands watched intact actors performing upper extremity motor tasks, but to date few have focused on intact participants watching prosthesis users. This scenario is important not only for the patient in the acute phase of amputation for initial training, but also prosthesis users in the chronic phase who observe and are observed executing motor actions every day.

Assessing the differences in brain activity when observing actions performed with a prosthesis compared to a hand would increase our understanding of the underlying cognitive processes in action observation, and whether the processes were the same, or different in either condition. Differences in brain activity would suggest that models developed by association of motor and sensory information are essential elements in the functioning of the action observation network.

4.2 Hypotheses

To gain further understanding of the action observation network and any differences between watching a hand perform a task and a prosthesis performing the same tasks, we developed the following goals. We sought to determine the neural activation differences of observing actions performed using a prosthesis, compared to those performed by a hand. Additionally,

we sought to assess differences in repetition suppression (see Section 2.3.1 on page 20) of brain activity in grasp-related neural areas when watching repeated presentations of videos of a hand or prosthesis performing the tasks. Finally, we wanted to determine if the end-effector used (prosthesis or hand) affected neural activation in sensory neural areas.

We hypothesize that an intact participant watching a hand perform grasping actions will result in greater repetition suppression of neural activity in grasp-related neural areas than will watching a prosthesis user. Secondly, when an intact participant observes interactions between an end-effector and an object, neural activation in sensory neural areas will be greater for hand-object interactions than for prosthesis-object interactions.

4.3 Methods

We used magnetic resonance imaging (MRI) to collect anatomical and functional images of participants. The use of MRI for both imaging modalities is well established in the literature. See the seminal work by Damadian (1971) and Frahm, Merboldt, and Hänicke (1993). The physical and physiological mechanisms of MRI were previously discussed in Section 2.3 on page 16, while repetition suppression is discussed in Section 2.3.1 on page 20.

4.3.1 Participants

Fifteen (age 18 to 47 years, 10 female) right-handed neurologically healthy adults participated in the study. All subjects provided written, informed consent, and all methods were approved by the Georgia Institute of Technology Institutional Review Board. Subjects read a list of contraindications for MRI and indicated their lack of contraindications. Subjects completed an MRI screening questionnaire and indicated 'no' to all pathologies. Subjects completed a health questionnaire which included assessment of handedness (Oldfield, 1971), eyesight, language/education, general health, and details of age, gender, date of birth, etc.

4.3.2 Stimuli and Experimental design

A repetition suppression (RS) paradigm was created based on previous work by Thioux and Keysers (2015). Upon initial presentation of a stimulus video, neural activity in brain areas sensitive to properties of the stimuli increases, thus increasing demand for blood (see Section 2.3 on page 16 for further detail). To meet the demand for oxygen, regional blood flow to the areas increases. It is proposed that with repeated presentation of stimuli with common properties, the regional cerebral blood flow (rCBF) of brain areas involved in processing the common properties will progressively suppress, or habituate. The RS phenomenon allows one to identify neural areas that are sensitive to, or not sensitive to, properties that are common among the repeated stimuli.

Presenting videos with two different end-effectors (hand and prosthesis), and objects with similar semantics (a cup for drinking) but different sensory properties (a paper cup and a ceramic cup) may result in differential activation of relevant cortical areas. Observation of these videos by intact people could reveal different brain processes used to assess action intent by the prosthesis actor and hand actor.

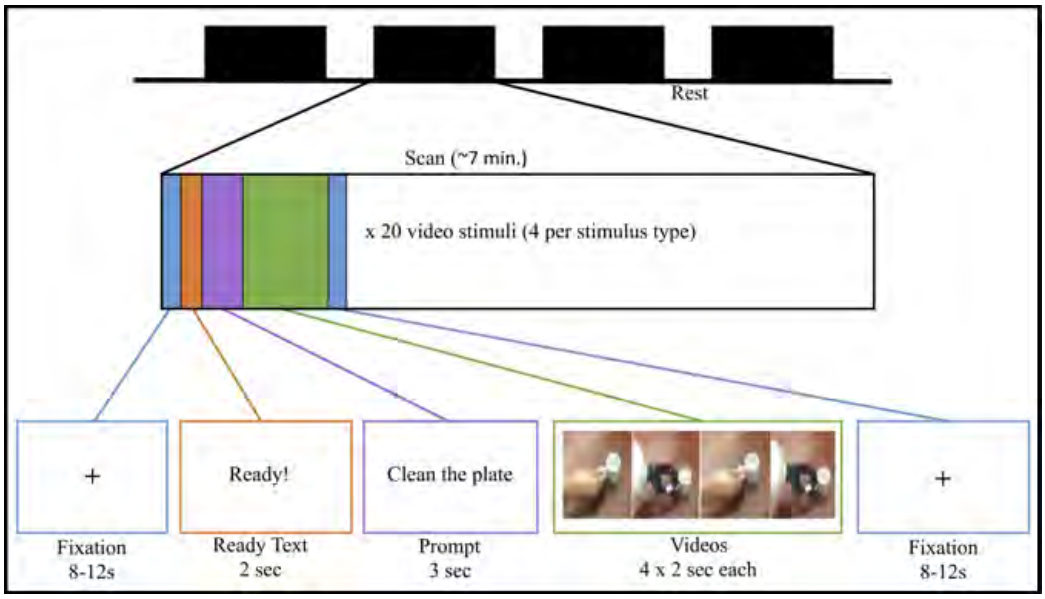

Figure 4.1: Experimental paradigm. Videos are presented in blocks of four two-second vignettes. Some blocks repeat the same video, and some alternate end-effector or object. Please see the text for a full description of stimuli and their groupings.

Stimuli were presented using PsychoPy 2 software (Peirce, 2008; https://www.psychopy.org) in four $7\,\mathrm{min}$ runs, with each run consisting of the presentation of 20 stimulus sets. Each set was composed of a fixation cross ($8\,\mathrm{s}$ to $12\,\mathrm{s}$), a ready prompt ($2\,\mathrm{s}$), a task prompt ($3\,\mathrm{s}$), and four concatenated videos of $2\,\mathrm{s}$ each (see Figure 4.1 on the preceding page). Task prompt text was salient to the object and task which was to be presented, for example, "Clean the plate" was displayed before video of reaching for a plate. In order to assess the effects of repetition suppression on brain areas, sets of videos consisted of the same video repeated four times, or of two different videos alternated twice. Alternating videos had either a different end-effector, or different objects with similar semantic meaning. The various stimuli sets were grouped into contrasts for statistical analysis of blood oxygen-level dependent (BOLD) and RS effects. The contrasts were: hand same object, hand alternating object, prosthesis same object, prosthesis alternating object, and alternating hand and prosthesis with the same object, all relative to fixation. Repetition suppression effects were assessed using contrasts of the first and last presentation of the video stimuli in each block.

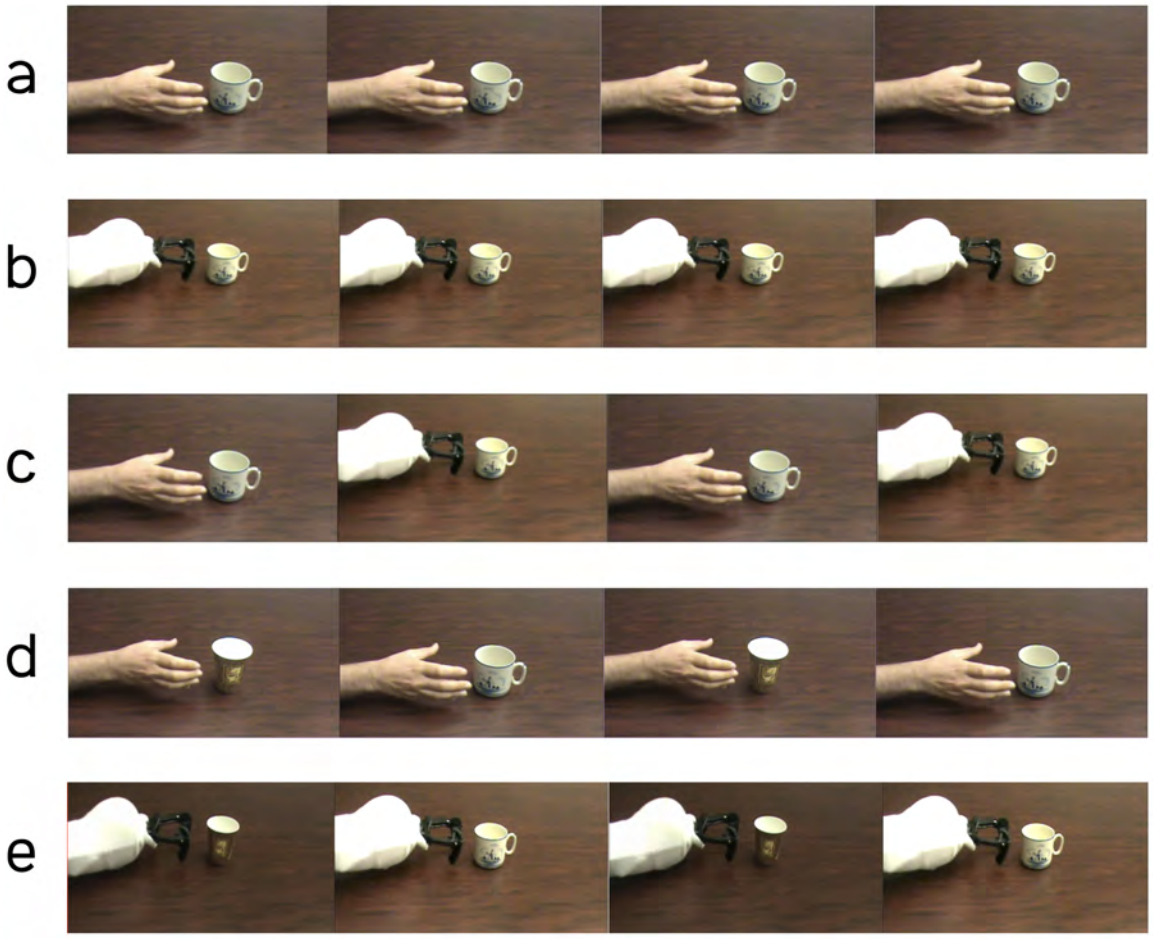

Figure 4.2: Exemplar blocks of video stimuli. (a) hand reaching for the same object. (b) Prosthesis reaching for the same object. (c) Alternating hand and prosthesis reaching for same object. (d) hand reaching for alternating object. (e) Prosthesis reaching for alternating object.

4.3.3 Data collection

Data were collected at the Georgia Institute of Technology / Georgia State University Center for Advanced Brain Imaging (Atlanta, Georgia, USA) using a Siemens (Washington, DC) TrioTim $3\,\mathrm{T}$ scanner with a 12 channel head coil. Three-dimensional structural volumes were acquired as T1-weighted images using a MPRAGE sequence (time-to-echo [TE]=$3.98\,\mathrm{ms}$, time-to-repetition [TR]=$2.25\,\mathrm{s}$, [TI]=$850\,\mathrm{ms}$, flip angle $9°$, FOV=$256\,\mathrm{mm} \times 256\,\mathrm{mm}$, 176 sagittal $1\,\mathrm{mm}$ slices, 256×256 matrix). T2*-sensitive functional imaging was performed

using a gradient-echo echo-planar-imaging sequence (time-to-echo [TE]=30 ms, time-to-repetition [TR]=2 s, 90° flip angle, field of view [FOV]=204 mm, 68×68 in-plane matrix, 37 axial 3 mm slices with 10% gap. β_0 unwarping, echo spacing was 0.49 ms, and phase encoding was A>P). In addition to structural and functional images, a field map was acquired (37 slices 3 mm thickness, TR=488 ms, TE1=4.92 ms, TE2=7.38 ms), as well as diffusion-tensor images (DTI) (2 mm slice thickness, 64 slices, TR=7.7 s, TE=85 ms).

Anatomical, functional, diffusion weighted, and field map images were converted from the digital imaging and communications in medicine (DICOM) standard (NEMA, (Association et al., 2003)) to the NIfTI image standard (Cox et al., 2004) and to the Brain Imaging Data Structure (BIDS) file structure (Gorgolewski et al., 2016) using `dcm2niix` (Li et al., 2016).

4.3.4 Preprocessing

Imaging data were preprocessed using workflows developed using `Nipype` (Gorgolewski et al., 2011b; RRID:SCR_002502). Nipype is a framework written in Python v3 (Van Rossum & Drake, 2009; https://www.python.org) that provides a layer of abstraction and a cohesive interface to underlying neuroimaging tools. In the following workflows, FSL refers to the FMRIB Software Library v6.0 (Woolrich et al., 2009; Smith et al., 2004; Jenkinson et al., 2012; https://fsl.fmrib.ox.ac.uk/fsl/fslwiki/), SPM is the Statistical Parametric Mapping toolset (Penny et al., 2011; https://www.fil.ion.ucl.ac.uk/spm/software/spm12/), while `rapidart` is provided by Nipype itself. Additionally, packages from the science stack for Python were used. These packages included `NumPy` (Harris et al., 2020; https://numpy.org), `Pandas` (McKinney et al., 2010; https://pandas.pydata.org), `NiBabel` (Brett et al., 2020; https://github.com/nipy/nibabel), nilearn (Abraham et al., 2014a; https://nilearn.github.io/stable/index.html), `PyBIDS` (Yarkoni et al., 2019; Yarkoni et al., 2021; https://bids-standard.github.io/pybids/), and `SciPy` (Virtanen et al., 2020; https://scipy.org), in addition to core Python packages. Processing was performed

using a custom Docker (Merkel, 2014; https://www.docker.com/) container based on the `nipype_tutorial` container (https://github.com/miykael/nipype_tutorial).

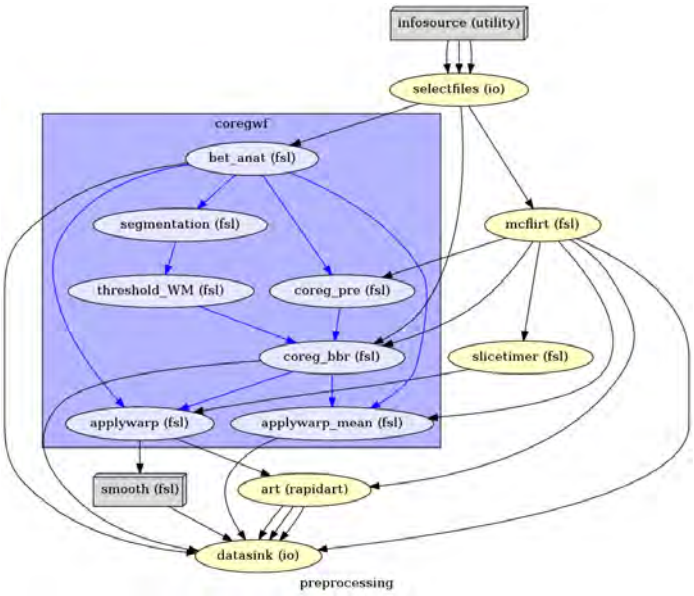

Figure 4.3: Workflow diagram for pre-processing structural and anatomical MR data using *Nipype*. Nodes represent processes in the workflow, while directional edges indicate data flow. Further details may be found in the text.

Anatomical data preprocessing

T1-weighted structural images were skull-stripped using the Brain Extraction Toolbox (BET) from FSL to remove non-brain tissue. These data were then segmented into grey matter, white matter, and cerebrospinal fluid areas using FMRIB's Automated Segmentation Tool (FAST), also from FSL. These data were thresholded (>50%) for white matter, after which they were co-registered with functional data as described in the *Functional data preprocessing* section.

Functional data preprocessing

T2*-weighted functional images were processed using FSL's motion correction library `MCFLIRT` (Jenkinson et al., 2002a). A three-dimensional mean image of the four-dimensional functional data for each run was then pre-aligned (using 6 degrees of freedom) with the

participant's anatomical image (from section *Anatomical data preprocessing*). Motion-corrected 4D data were slice time corrected to the mid-point of the TR time to account for the acquisition time ($2\,\mathrm{s}$) of each volume. Functional mean and pre-aligned anatomical images, as well as motion correction parameters were then submitted to a registration routine which used a boundary-based registration. The co-registration warp parameters were then applied to the functional images, as well as the mean functional image. Functional data were processed using `rapidart` to find artifacts due to variations in luminance or subject motion. Functional data were smoothed with a $5\,\mathrm{mm}$ full-width at half-maximum (FWHM) Gaussian kernel.

4.3.5 First-level statistical analyses

First-level statistical processing calculates beta weights for each explanatory variable within each subject. Pre-processed anatomical and functional images were entered into a workflow for first-level analyses (see Figure 4.5 on page 56). Contrasts were defined for fixation, the ready prompt, the task prompt, and the stimuli presentations as shown in Figure 4.2 on page 50 and previously discussed in Section 4.3.2 on page 48. The design matrix is shown in Figure 4.4 on page 55. A list of explanatory variables and their contrasts are shown in Table 4.1 on the next page. Explanatory variables were entered into a generalized linear model to obtain beta weights. BOLD responses were obtained by comparisons of beta weights during viewing stimuli with beta weights during the fixation period. Suppression effects were assessed by comparing the beta weights of the first and fourth presentations of stimuli within a block. Beta values lower in the fourth presentation are indicative of repetition suppression.

First-level processing was performed in subject space to minimize artifacts due to transformation of 4D functional data to MNI space (Wu et al., 2011). After first-level processing, resulting beta images were transformed to MNI space for subsequent second-level analyses. This workflow is depicted in Figure 4.6 on page 56.

Explanatory Variables
Fixation
Ready Text
Prompt Text
IntactProsAlt1, IntactProsAlt2, IntactProsAlt3, IntactProsAlt4
IntactAltObj1, IntactAltObj2, IntactAltObj3, IntactAltObj4
IntactSame1, IntactSame2, IntactSame3, IntactSame4
ProsAltObj1, ProsAltObj2, ProsAltObj3, ProsAltObj4
ProsSameObj1, ProsSameObj2, ProsSameObj3, ProsSameObj4

(a) Explanatory variables

Contrasts
Intact Suppression
Prosthesis Suppression
Alternating End Effector Suppression
Alternating Object Suppression
All Same Object > Fixation
All Alt Object > Fixation
Intact > Fixation
Pros > Fixation
Intact > Prostheses
Pros > Intact
All Same Object > All Alt Object
All Alternating Object > All Same Object
Alt object suppression for intact
Alt object suppression for prosthesis

(b) Contrasts

Table 4.1: a) Explanatory variables were entered into a generalized linear model to obtain beta weights. b) Statistical differences of beta weights were obtained and contrasts of those weights entered into first-level analyses for each participant, then into second-level group analyses.

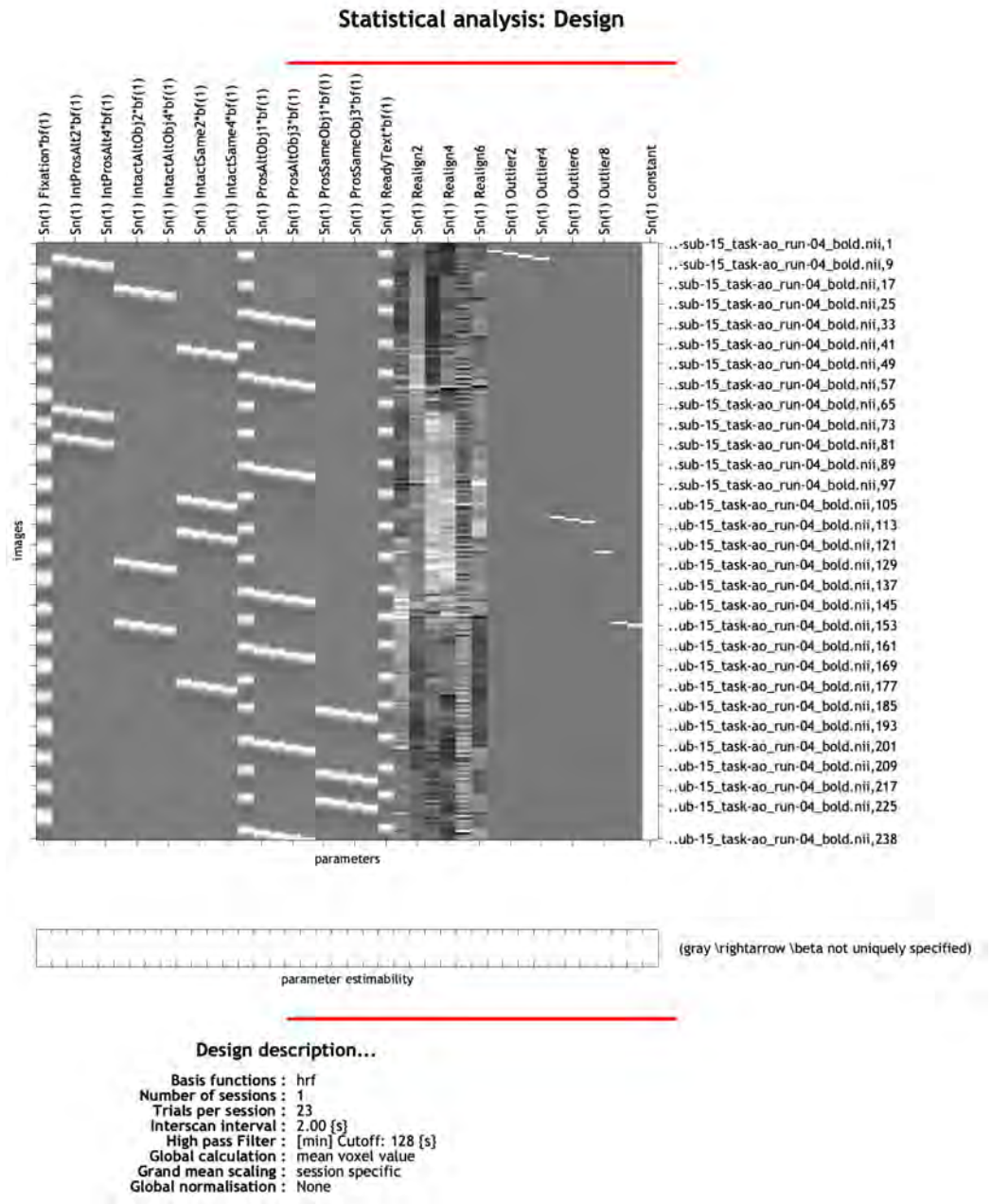

Figure 4.4: Statistical design showing explanatory variables (some named along the top of the matrix) which have been convolved with the hemodynamic response function. In addition to defined explanatory variables, variables for confounds such as realignment and outliers due to head motion are also incorporated into the design. Along the vertical axis are the 238 volumes captured for exemplar subject 15.

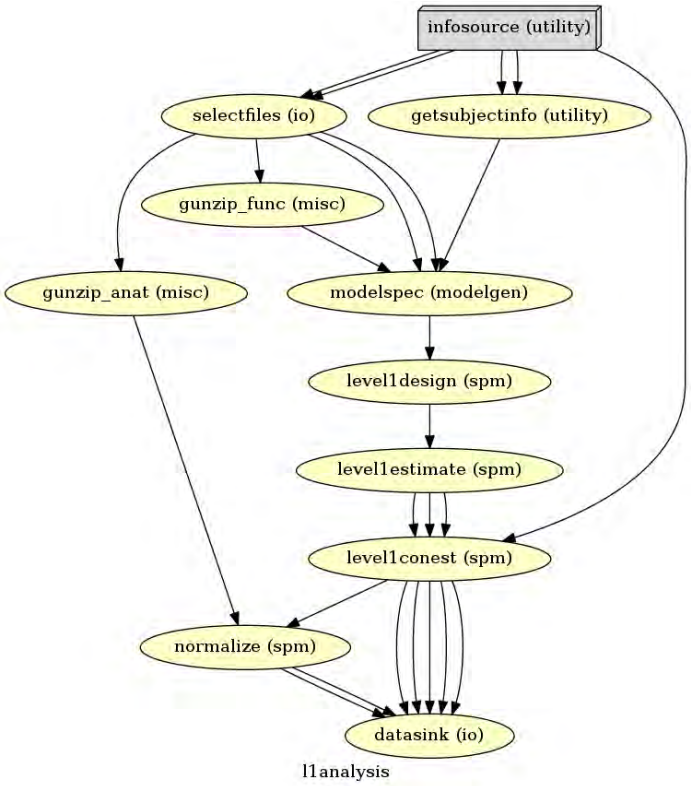

Figure 4.5: First-level (individual subject) processing of pre-processed data. See the text for a detailed explanation.

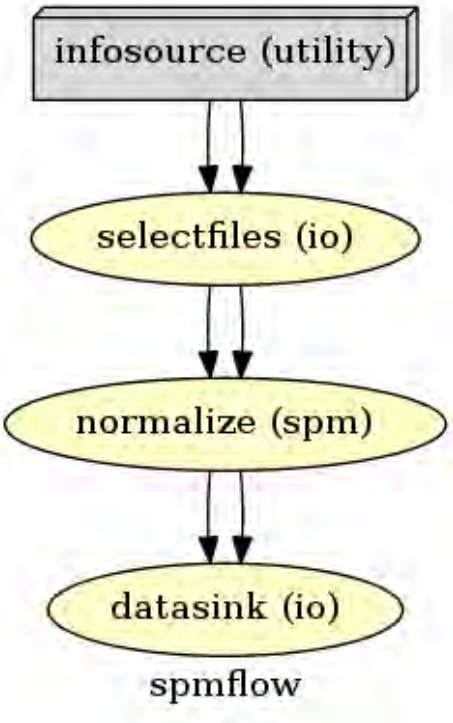

Figure 4.6: Workflow for transforming first-level statistical results from subject-space to MNI-space.

4.3.6 Second-level analyses

Results from the individual analyses performed in the first-level analyses were entered into a workflow (Figure 4.7) to obtain group-level statistical results. Resulting t-images were thresholded at $p < 0.005$ using false discovery rate correction and clustered with a minimum cluster size of 5 voxels. The resulting clusters were then thresholded at $p < 0.05$ to obtain final t-images. Thresholded t-images were visualized using `Surf Ice` (https://www.nitrc.org/projects/surfice). MNI coordinates for cluster peak activations were obtained using `AtlasReader` (Notter et al., 2019; https://github.com/miykael/atlasreader). Brain regions were obtained using the Jülich Atlas (Eickhoff et al., 2005; https://www.fz-juelich.de/de/inm/inm-1), Automated Anatomical Labelling Atlas 3 (Rolls et al., 2020; https://www.gin.cnrs.fr/en/tools/aal/), the Harvard-Oxford Atlas (Desikan et al., 2006; http://www.cma.mgh.harvard.edu/), and the Yale BioImage Suite Package (Lacadie et al., 2008; https://bioimagesuiteweb.github.io/webapp/mni2tal.html).

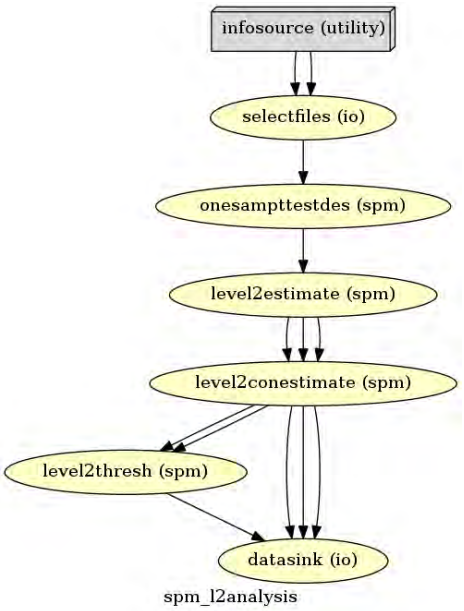

Figure 4.7: Workflow of second level (group) analysis of first-level data.

4.4 Results

We sought to test our hypothesis that grasp-related areas would be differentially activated when observing a hand reaching for objects, compared to a prosthesis reaching for objects. Additionally, we tested our hypothesis that sensory areas would demonstrate differences in activation when observing a prosthesis reaching for objects versus a hand reaching for objects.

4.4.1 BOLD activations when watching a hand or prosthesis

As expected, when viewing video stimuli large activations are present throughout bilateral visual cortices, confirming basic validity of the paradigm. Areas of particular interest are the activations along the inferior frontal sulcus in the intact condition, extending to Brodmann Areas 44, 45, and 46, which are dramatically reduced in the prosthesis condition. Similarly, there is greater left supramarginal/angular gyrus activation in the intact condition (see Figures 4.8a to 4.8d and Table 4.2 on page 60 and on page 62).

4.4.2 Differences in BOLD activations when watching a hand and prosthesis

Figures 4.9a to 4.9d and Table 4.2 on pages 61–62 show areas with activations higher when observing the hand than when observing the prosthesis or higher when observing prosthesis versus the hand. Notable among these differences are the left anterior dorsal activity in Figure 4.9a on page 61, and the differences in Brodmann Area 46, the insular cortex, and supramarginal and parietal areas in the right hemisphere Figure 4.9b on page 61.

4.4.3 Repetition suppression when watching alternating objects

Areas with statistically significant repetition suppression effects when a hand and prosthesis reach for alternating objects are shown in Figure 4.11 on page 65. Notable differences are found in the left hemisphere with greater suppression in supramarginal gyrus, inferior

parietal lobule, Brodmann area 44.

4.4.4 Repetition suppression when watching alternating objects compared to repeating same objects

Comparing presentations of alternating object and same object, greater activation viewing same object than alternating object is seen in left angular gyrus, inferior parietal lobule, and visual association areas (see Table 4.3 on page 63). Greater activation for alternating object compared to same object are not seen.

4.4.5 The effect of end-effector on repetition suppression while observing alternating objects

Suppression effects for alternating object when the end-effector is a hand are shown in Figures 4.11a and 4.11b on page 65 and include primary and secondary visual, frontal eye fields, BA44, BA45, IPL, IPS, premotor, and angular gyrus areas. Different patterns of suppression are seen when the prosthesis is the end-effector reaching for the objects, and are shown in Figures 4.11c and 4.11d on page 65. Areas include primary and secondary visual, supramarginal gyrus, IPL, IPS, angular gyrus, supramarginal gyrus, premotor, and supplementary motor areas.

Noticeable differences between intact suppression and prosthesis suppression include greater suppression in superior parietal lobule extending to inferior parietal lobule and along the post-central sulcus in the left hemisphere. In the right hemisphere, greater suppression is seen along the inferior frontal sulcus including Brodmann areas 44 and 45. Greater suppression in the prosthesis condition is seen along the intraparietal sulcus extending from the superior parietal lobule to the occipital lobe in the right hemisphere.

4.4.6 BOLD activations and differences

Intact and prosthesis, same objects

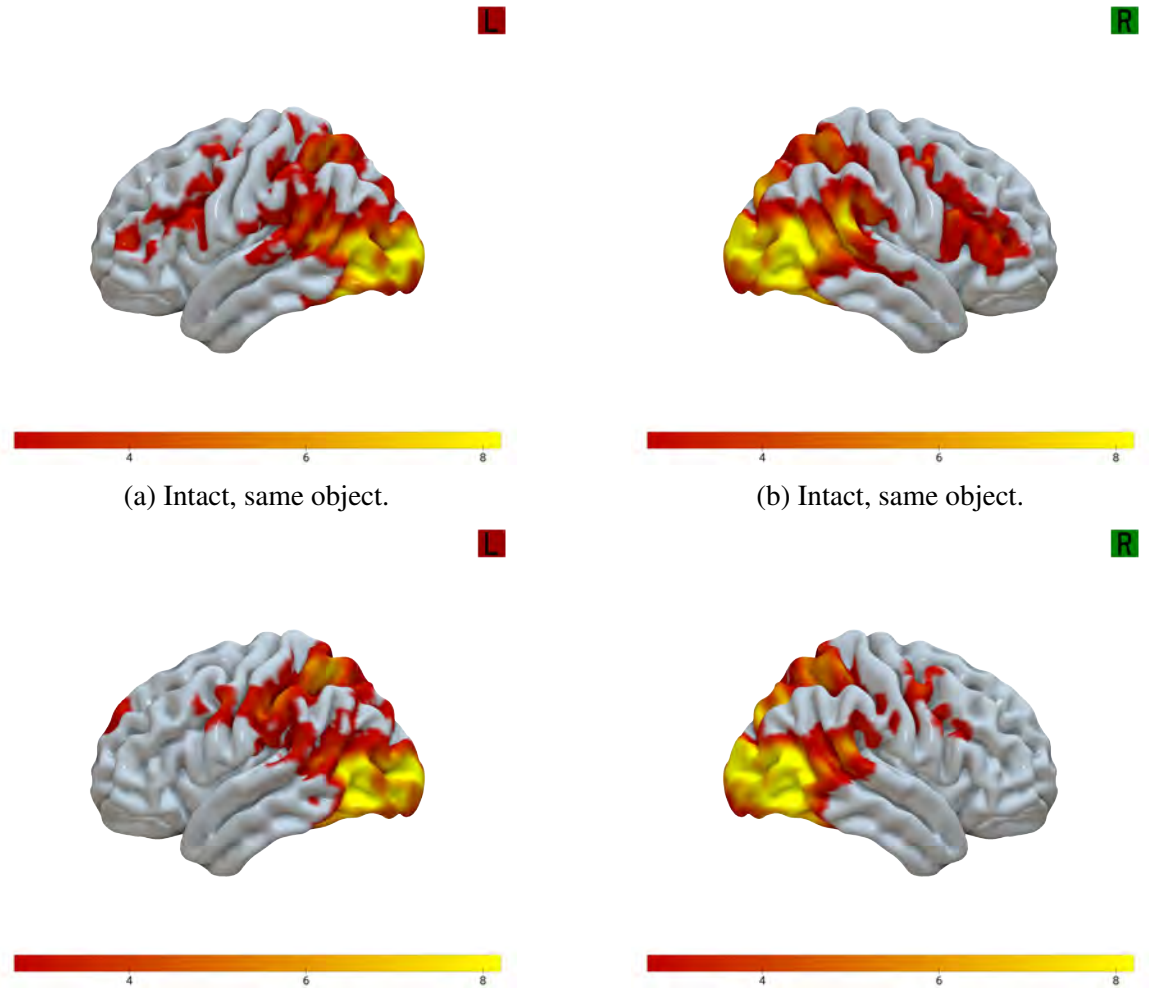

(a) Intact, same object.

(b) Intact, same object.

(c) Prosthesis, same object.

(d) Prosthesis, same object.

Figure 4.8: Blood oxygen-level dependent response when observing video stimuli. Activity statistically significantly greater than fixation while observing intact are shown in (a) and (d), while activity while watching prosthesis are shown in (b) and (e). Areas with activations statistically significantly higher in intact than prosthesis are shown in subfigures (c) and (f). Notable among these differences are the left anterior dorsal activity in (c), and the differences in Brodmann Area 46, the insular cortex, and supramarginal and parietal areas in the right hemisphere (f). Please refer to Table 4.2 on page 62 for coordinates of peak cluster activations.

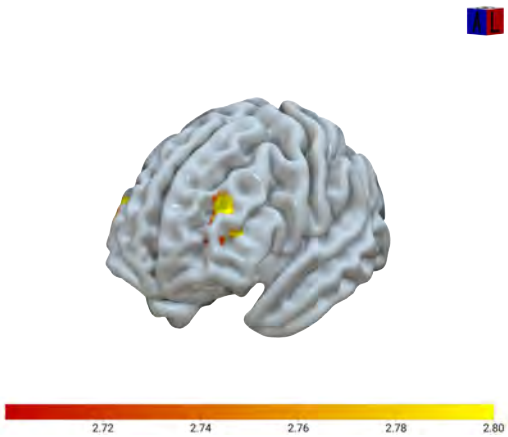

(a) Intact greater than prosthesis.

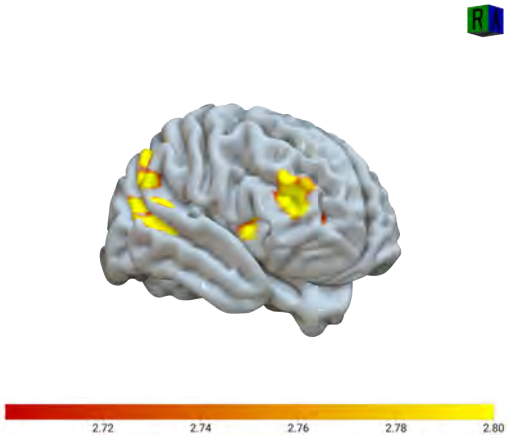

(b) Intact greater than prosthesis.

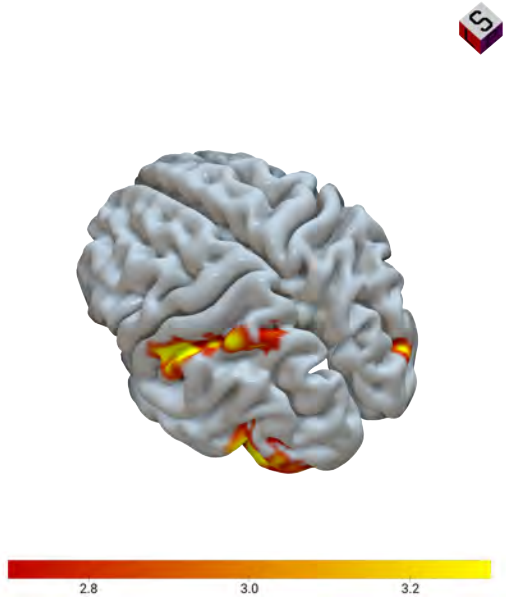

(c) Prosthesis greater than intact.

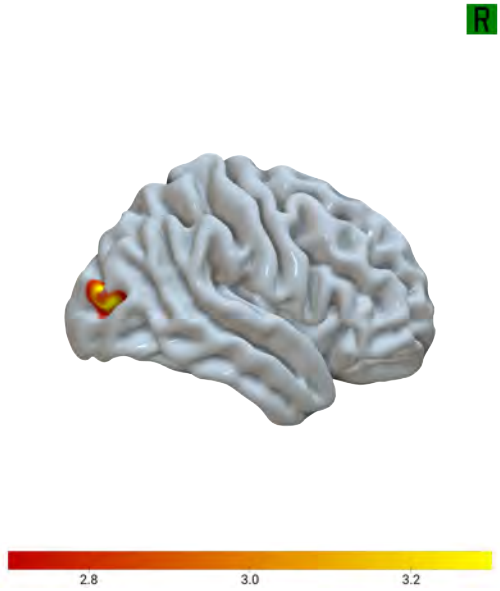

(d) Prosthesis greater than intact.

Figure 4.9: Areas with activations statistically significantly higher in intact than prosthesis are shown in subfigures (a) and (b). Notable among these differences are the left anterior dorsal activity in (a), and the differences in Brodmann Area 46, the insular cortex, and supramarginal and parietal areas in the right hemisphere (d). Areas with activations statistically significantly higher in prosthesis than intact are shown in subfigures (c) and (d). Notable are the activations in areas of anterior superior and inferior parietal lobules (c) and lateral occipital cortex in the right hemisphere (d). Please refer to Table 4.2 on the next page for coordinates of peak cluster activations.

Activation

Condition	X	Y	Z	Brain Region	Brodmann Area
Intact > fixation					
	24	-96	4	R Secondary visual	18
	47	0	52	R Premotor, supplementary motor	6
	-34	-1	44	L Premotor, BA44	6, 44
	29	1	-1	R Putamen	
	-8	-72	-36	L Cerebellum 7b	
	23	-29	-2	R Hippocampus dentate gyrus, Thalamus	
	-39	49	10	L Dorsolateral prefrontal cortex	46
	-22	-37	67	L Primary sensory	1
Prosthesis > fixation					
	52	-70	1	R Fusiform Gyrus	37
	55	-1	49	R Premotor	6
	-9	-73	-39	Cerebellum 7b	
	-53	6	45	L Premotor, supplementary motor	6
	-10	59	31	L Anterior prefrontal cortex	10
	22	-29	-2	R Hippocampus dentate gyrus, Thalamus	
	55	-50	-28	R Inferior temporal gyrus	20
	1	59	33	R Frontal pole	
Intact > prosthesis					
	43	-49	46	R Supramarginal gyrus, Angular gyrus, IPL PFm	40
	56	-44	10	R Superior temporal gyrus, Angular gyrus, IPL Pga	22
	41	43	8	R Dorsolateral prefrontal cortex	46, 45
	-8	-96	26	L Secondary visual	18
	31	7	-1	R Putamen, Insula	
	-31	38	28	L Anterior prefrontal cortex	10
	14	-70	5	R Primary visual	17
	8	-70	18	R Primary visual	17
	-26	-8	10	L Putamen, Insula	
	25	-65	18	R Visual cortex	18
	-36	33	13	L Dorsolateral prefrontal cortex, BA44, BA45	44, 45, 46
Prosthesis > intact					
	-47	-68	-5	L Visual association	19
	-54	-29	39	L Supramarginal gyrus, IPL PFt, IPL PF	40
	-41	-45	65	L SPL 7A, SPL 7PC, Primary somatosensory cortex	2
	39	-82	10	R Visual association	19

Table 4.2: MNI coordinates of peak activation of clusters, brain regions of the peaks, and Brodmann areas (if defined) for stated conditions. Please refer to the images in Figures 4.8 and 4.9 on page 60 and on the previous page, as well as the text for further descriptions.

Activation comparisons for alternating object and same object

Activation for alternating object compared to same object

Condition	X	Y	Z	Brain Region	Brodmann Area
Same > Alternating					
	-50	-56	37	L Angular gyrus, IPL Pga, IPL PFm, IPS hIP1, IPL PGp	39
	-40	-75	29	L Angular gyrus, IPL PGp	39
	-1	-87	33	L Visual association, V2, SPL 7P	18, 19
Alternating > Same					
				none	

Table 4.3: MNI coordinates of peak activation of clusters, brain regions of the peaks, and Brodmann areas (if defined) for stated conditions.

Same objects versus alternating objects

4.4.7 Repetition suppression effects

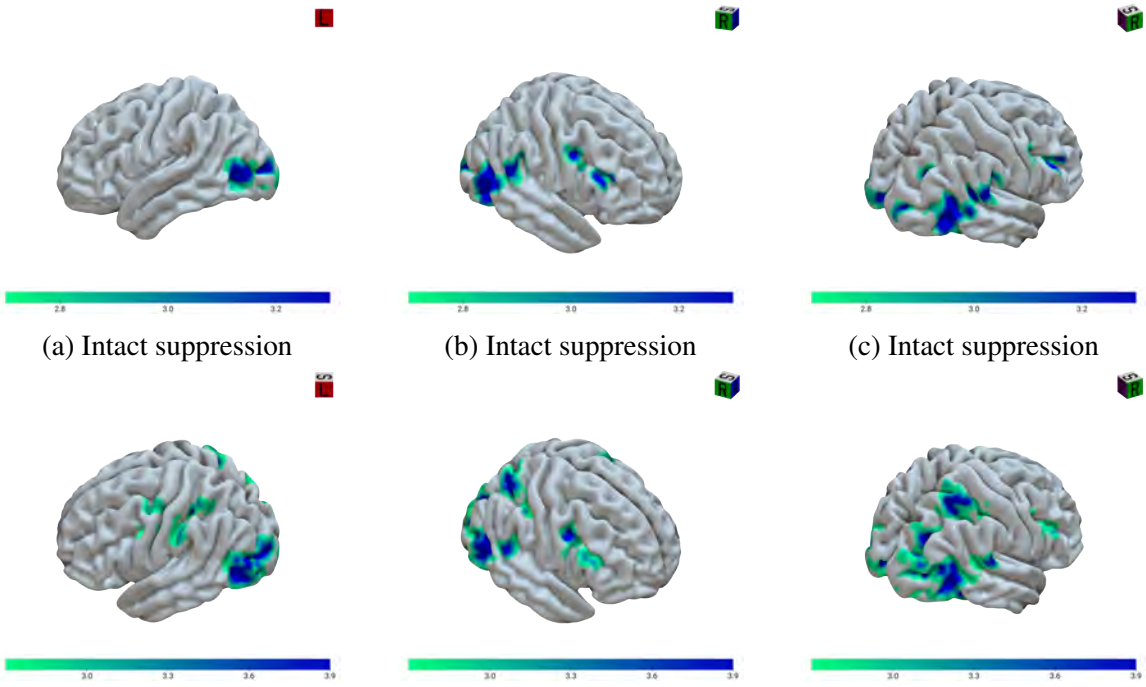

(a) Intact suppression (b) Intact suppression (c) Intact suppression

(d) Prosthesis suppression (e) Prosthesis suppression (f) Prosthesis suppression

Figure 4.10: Brain areas exhibiting repetition suppression when observing videos of either repeating hand reaching for an object (a-c), or prosthesis reaching for an object (d-f). Cluster peak information may be found in Table 4.4 on the next page.

Repetition Suppression

Condition	X	Y	Z	Brain Region	Brodmann Area
Intact					
	16	-89	-3	R Primary visual, secondary visual	17, 18
	-19	-93	3	L V3V, V4, V2, secondary visual	18
	-47	-73	5	L V5, Visual association	19
	45	5	36	R BA44, Premotor	44, 6
	47	24	21	R BA45, Dorsolateral Prefrontal Cortex	9
	31	-79	34	R Angular Gyrus, IPL PGp	39
	33	-57	-19	R Fusiform Gyrus	37
Prosthesis					
	15	-92	-4	R Primary Visual, V1, V2, V4, V5	17
	-15	-92	-5	L Primary Visual, V3V, V4, V5	17
	25	-56	51	R Visuomotor, SPL 7A, SPL 7PC, IPS hIP3	7, 2
	-55	-27	43	L Supramarginal Gyrus, IPL PFt, IPL PF	40, 1, 2
	-45	-5	43	L Premotor + Supplemental Motor	6
	47	4	34	R BA46, BA44, Premotor, Supp. Motor	46, 44, 6
	-28	-46	50	L Visuomotor, BA2, IPS hIP3, SPL 7PC	2, 7
	56	12	28	R Ventral Premotor, BA44, BA45	44, 45
	-39	-43	57	L Visuomotor, BA2, SPL 7PC, IPS hIP3, BA1	2, 7, 1
	-48	3	29	L Premotor, BA44, Supplemental Motor	6, 44
	-54	-73	-9	L Visual Association Area	19

Table 4.4: MNI coordinates, brain regions, and Brodmann areas (if defined) for areas of repetition suppression when observing videos of either repeating hand reaching for an object, or prosthesis reaching for an object. Please refer to Figure 4.10 on the previous page for spatial visualization of suppression effects.

Intact vs Prosthesis alternating object suppression

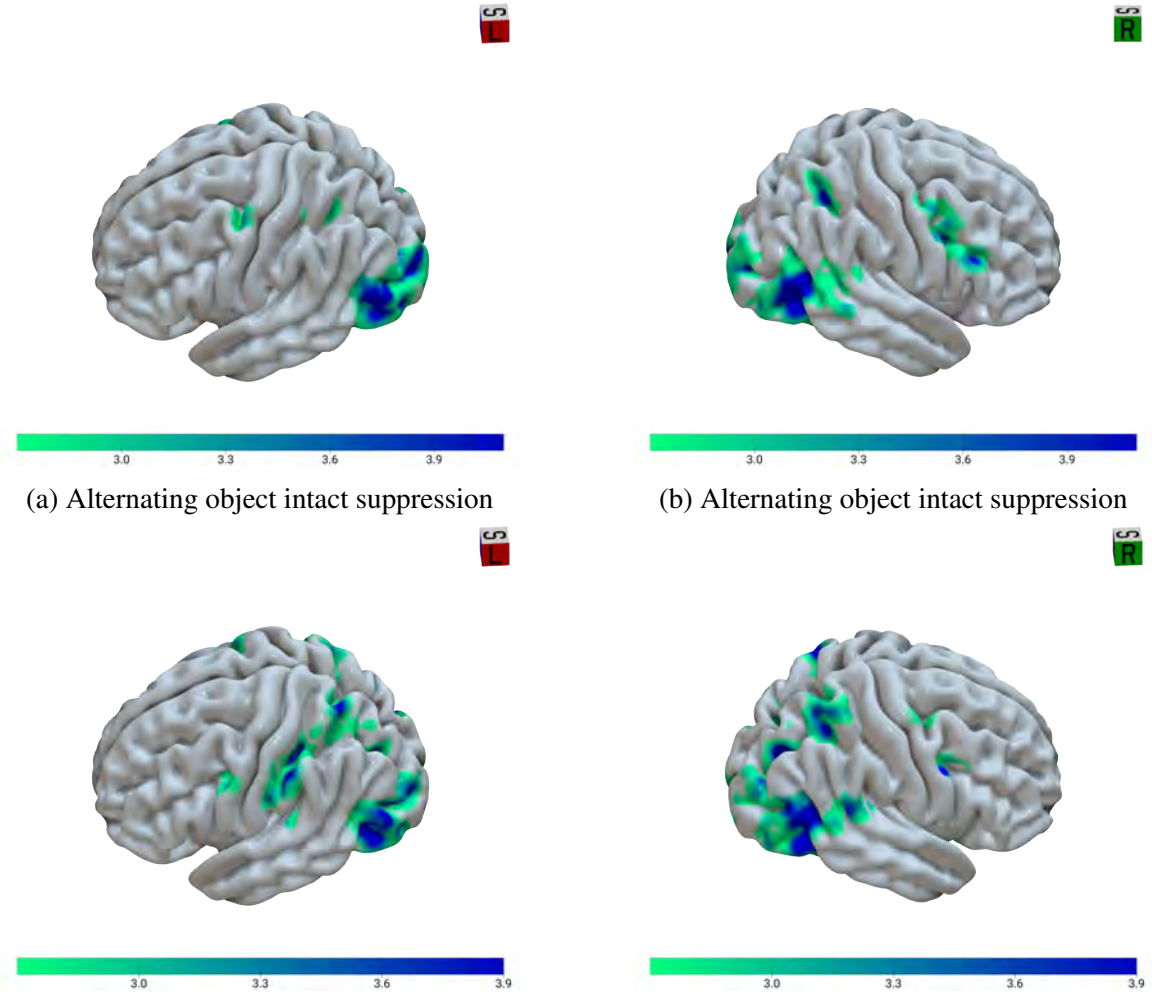

(a) Alternating object intact suppression

(b) Alternating object intact suppression

(c) Alternating object prosthesis suppression

(d) Alternating object prosthesis suppression

Figure 4.11: Brain areas exhibiting repetition suppression when observing videos of alternating object (such as paper cup, stoneware mug) when being reached for by either the hand or the prosthesis. Cluster peak information is available in Table 4.5 on the next page.

Condition	X	Y	Z	Brain Region	Brodmann Area
Intact					
	16	-94	-3	R Primary visual	17
	-15	-90	-8	L Secondary visual	18
	46	9	41	R Frontal eye fields, BA44, BA6	8, 6
	43	24	18	R Dorsolateral prefrontal cortex, BA45, BA44	9, 45, 44
	29	-53	48	R Visuomotor, SPL 7A, IPS hIP3, IPL PF	7
	47	-40	14	R Superior temporal gyrus, IPL Pga, IPL PFm, IPL PF	22
	-26	-51	48	L Visuomotor, IPS hIP3, BA2, SPL 7PC, SPL 7A, SPL 5L, IPS hIP1	7
	-44	-5	56	L Premotor, supplementary motor,	6
	48	-54	19	R Angular gyrus, IPL PGp, IPL Pga	39
Prosthesis					
	15	-93	-3	R Primary visual	17
	-23	-87	-12	L Secondary visual	18
	-58	-27	46	L Supramarginal gyrus, IPL PFt, BA2, IPL PF, IPS hIP3	40
	-26	-57	66	L SPL 7A, IPS hIP3, SPL 7PC, BA2	2
	28	-55	49	R Visuomotor, SPL 7A, IPS hIP3, SPL 7PC	
	61	-45	25	R Angular gyrus, IPL PFm, IPL PF, IPL Pga	39
	-26	-70	30	L SPL 7A, IPS hIP3	
	-52	1	34	L Premotor, supplementary motor, BA44, BA6	44, 6
	47	6	34	R Premotor, supplementary motor, BA44, BA6	44, 6
	-54	-26	17	L Supramarginal gyrus, sec. somatosensory cortex, parietal oper. OP1, IPL PFop	40
	36	-6	63	R Premotor, supplementary motor	6
	-26	-80	-5	L Secondary visual	18
	54	-56	6	R Fusiform, IPL PGp	37

Table 4.5: MNI coordinates, brain regions, and Brodmann areas (if defined) for areas of repetition suppression when observing videos of either. Please refer to Figure 4.11 on the previous page for spatial visualization of suppression effects.

4.5 Discussion

While subjects watched the hand reaching for objects, there were BOLD activations above baseline in visual areas, and along bilateral inferior frontal sulci including areas of the ventral premotor cortex (Brodmann Areas 44, and 45). There were also activations of cortical areas in the bilateral supramarginal/angular gyrus, bilateral superior temporal sulci, and bilateral superior and inferior parietal lobules. These areas of activation comprise areas associated with visual processing and with the action observation network (Kilner, Friston, & Frith,

2007). These results suggest recruitment of the action observation network when watching a hand reaching for objects.

When subjects watched the prosthesis reaching for objects, the BOLD activations above baseline were in bilateral visual, superior and inferior parietal lobules, supramarginal/angular gyri, as well as left sensory and motor areas, and right inferior frontal junction area. The activations of visual, supramarginal/angular gyrus, and parietal areas, but the near absence of premotor activation along the inferior frontal sulci suggest recruitment of some of the action observation network areas. The absence of activation of premotor areas may suggest the naïve observers' lack of available associations of kinematics and motor commands for the prosthesis.

Greater activation for repeated presentations of the same object vs. alternating object in left angular gyrus, inferior parietal lobule and intraparietal sulcus suggest increased recruitment of these areas to assess object properties and object affordances (Bach, Nicholson, & Hudson, 2014; Mizelle, Kelly, & Wheaton, 2013). These effects are expanded upon using repetition suppression data for hand reaching for alternating objects, vs prosthesis reaching for alternating objects as shown in Figure 4.11 on page 65. Here we see a similar effect of prosthesis use where inferior parietal lobule, superior parietal lobule, and angular gyrus suppression suggest a decreased ability to predict sensory consequences when viewing the prosthesis interacting with alternating objects (Saygin et al., 2012; Urgen, Pehlivan, & Saygin, 2019). These effects are similar to those seen in prosthesis reaching for the same objects as shown in Figure 4.10 on page 63.

Greater activity for observing intact compared to prosthesis in the right insula (see Figure 4.9b on page 61) was unexpected. Previous work by Di Cesare et al. (2016) and Di Cesare et al. (2021) showed that the affect of the observed actor's motor movements are modulated by their insula based on homeostatic, and the affect of their movements is evaluated in the insula of the observer. The present results suggest a difference in the observer's ability to assess the affect of the person performing the action with a prosthesis.

While our study design does not directly address this phenomena, the present results suggest further research in this area is warranted.

These results do not support our first hypothesis that an intact participant watching an intact actor perform grasping actions will result in greater repetition suppression of neural activity in grasp-related neural areas than will watching a prosthesis user. In fact, the opposite effect was shown in the posterior aspect of the right hemisphere (see Figure 4.10f on page 63) where repetition suppression was higher in superior parietal areas while watching repeated presentations of prosthesis reaching. This may be due to a lack of prior experience with the prosthesis, and thus a lack of prior sensory experience which led to a decreased ability of the action observation network to predict the sensory consequences of the observed actions. This informational deficit may then have led to suppression in the inferior parietal lobule and intraparietal sulcus as demonstrated by (Saygin et al., 2012).

Our second hypothesis that neural activation in sensory neural areas will be greater for hand-object interactions than for prosthesis-object interactions was supported by the present results in the right hemisphere (compare Figures 4.9b and 4.9d on page 61). Sensory areas in the left hemisphere did not show this effect, but instead showed an opposite effect of increased activation along the precentral sulcus (compare Figures 4.9a and 4.9c on page 61). This increased precentral activation along with activation in left visual areas (BA19, hMT/V5) may represent left-lateralized motor attentional activity and motion processing (Rushworth, Krams, & Passingham, 2001; Kaas et al., 2010).

4.6 Conclusions

The results of this study support a hypothesis of cognitive processing observed prosthesis use being fundamentally different than cognitive processes involved in observing hand actions. These effects were seen in premotor areas of the action observation network, as well as the insula which is part of a neural circuit that encodes the affect of observed actions. These results suggest that when observing actions executed with a prosthesis, there is

reduced ability to assess the kinematics of the movement. This deficit cascades to a reduced ability to assess the motor actions that would produce those kinematics, and ultimately the intention that would lead to those motor actions (see Chapter 1 on page 1 for an overview). Additionally, in neural circuits specialized to assess vitality of movements, a potentially important reduced response while watching the prosthesis compared to watching the hand was seen. Studies of brain activation provide important insights into the cognitive processes while performing tasks of interest. Changes in information flow and network development during these tasks can provide other insights not apparent from activation studies. Potential effective connectivity changes within these networks and changes of network properties are the subject of the connectivity analyses in Chapter 5 on the next page.

CHAPTER 5
SPECIFIC AIM 3

5.1 Introduction

Our previous study reported in Chapter 4 showed differences in activation of cortical areas associated with the action observation network while watching either a prosthesis or a hand performing reach-to-grasp tasks. These changes in activity may be indicative of changes not only in the amount of neural activation, but also changes in the effective connectivity between the brain areas. Decreased activity in areas of the action observation network specialized for determining intention from observed kinematics may indicate changes in informational processing from localized within network nodes to more dispersed between nodes. These network changes would be reflected in changes of network metrics such as the clustering coefficient of the network nodes (see Section 5.1.2 on the following page for an overview). To better understand any changes in effective connectivity and related changes in network properties, we performed connectivity and network theory analyses between regions of interest (ROI) defined by areas of peak cluster activation obtained in Aim 2.

5.1.1 Effective connectivity

Effective connectivity measures the direct influence brain areas have on other brain areas, and removes the influence of other factors, such as simultaneous activity due to stimulus presentation. This is in contrast to functional connectivity, which measures statistical dependencies of activity between brain areas based on the correlational similarity of their responses to stimuli (Friston, 2011). Thus, effective connectivity measures directed causal influence, and allows statistical comparisons between models of network activity and hypothesis testing of model differencs (Friston, 2011).

5.1.2 Network-theoretic measures

The clustering coefficient of a node is a measure of the local integration or connectedness of a node with its local subgraph of neighboring nodes (Rubinov & Sporns, 2010). Considering a node with k neighbors, there can be at most $k(k-1)/2$ edges between them (Watts & Strogatz, 1998). When nodes are connected with no randomization, the resulting network is highly clustered, and considered "large world". A network with completely random edges is poorly clustered and considered "small world". Ideal connectivity (high clustering with short path lengths) lies between the two extremes, and in biological systems is commonly found at a randomness probability of $p = 0.15$. See Figure 5.1 for a visualization. This small-worldness represents optimal tradeoff between path length through local nodes, while ensuring connectivity with other nodes within the network is not lost. The clustering coefficient for a network may be calculated as the mean of the clustering coefficients of the nodes within the network.

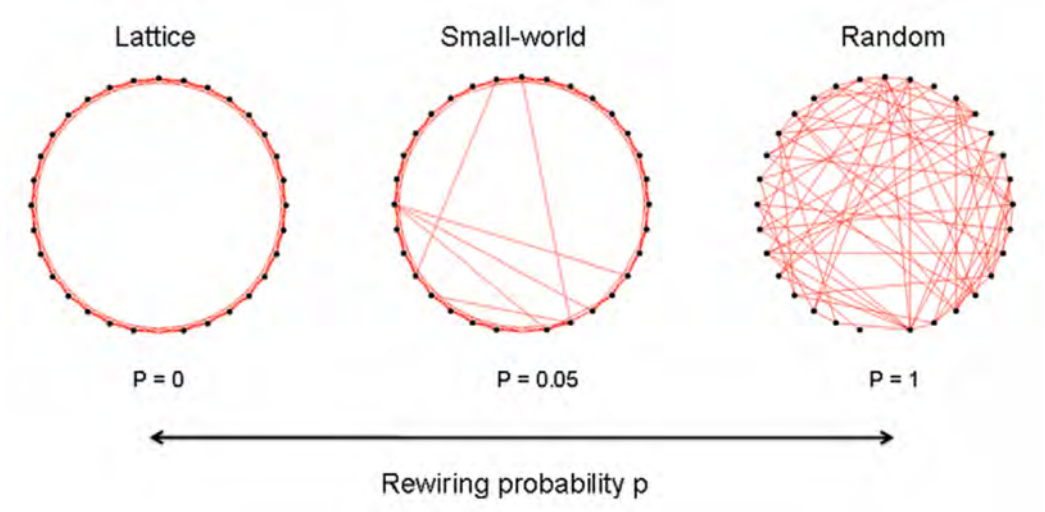

Figure 5.1: Graphical representation of network topology with varying degrees of rewiring probability. No randomness ($p = 0$) results in a lattice, where path lengths between nodes can be very long. High randomness ($p = 1$) results in a random network with short path lengths, but low clustering. Small-world networks (high clustering, short path lengths) occur with intermediate probabilities. In biological networks, this is commonly at randomness $p = 0.15$

5.2 Hypotheses

We hypothesized that watching the prosthesis perform reach-to-grasp tasks would result in decreased effective connectivity of brain areas comprising the action observation network compared to watching the hand perform the same tasks. We also hypothesize that network properties will reflect more global, rather than local, information flow in the prosthesis condition than in the intact condition.

5.3 Methods

5.3.1 Participants, Stimuli and experimental design, Data collection

The data collected for the BOLD-based analyses conducted in Aim 2 were used as the source data for the analyses conducted for the present Aim. For details, please see Chapter 4 on page 45.

5.3.2 Preprocessing

Preprocessing with fMRIPrep

The neuroimaging data used in Aim 2 were also used for this study. Preprocessing of the data was performed using fMRIPrep. A detailed description of the workflow is provided in Appendix A.

Preprocessing with `Conn` toolbox

Structural and functional volumes, tissue masks, confound regressors, and quality control covariates created by preprocessing with fMRIPrep were imported into the `Conn` toolbox (Whitfield-Gabrieli & Nieto-Castanon, 2012; https://web.conn-toolbox.org/home). Data were denoised at the voxel level for each participant using ordinary least squares regression to remove confounding variables. Data were further processed using component-based noise correction of noise from white matter and cerebrospinal areas (Behzadi et al., 2007a),

subject motion estimations (Friston et al., 1996), outlier scans (Power et al., 2014a), and session and constant task-induced effects (Whitfield-Gabrieli & Nieto-Castanon, 2012). The BOLD signal was then high-pass filtered with cutoff $0.008\,\mathrm{Hz}$ to minimize low frequency noise, such as scanner drift.

5.4 Analyses

5.4.1 ROI Definition

Clusters were extracted from thresholded T-statistic images for Intact > Fixation and Prosthesis > Fixation generated in Aim 2. MNI coordinates for cluster peak and subpeak activations were obtained using `get_peak_data` (Notter et al., 2019; https://github.com/miykael/atlasreader) with probability threshold 5, and minimum distance 50. Peaks within $10\,\mathrm{mm}$ were merged, and their center used as the coordinates (see Table 5.1 on the next page). Spheres of radius $8\,\mathrm{mm}$ were created at each coordinate using `create_sphere` from the `nltools` (Chang et al., 2021; https://nltools.org) package. Each of these spheres were used as ROI for the present analysis.

ROI-to-ROI effective connectivity

First-level effective connectivity between defined ROI was measured using a weighted general linear model with multivariate regression and using a weighted hrf (hemodynamic response function) (Nieto-Castanon, 2020; Ceravolo et al., 2021). Connectivity between pairs of ROI is measured, while controlling for effects of other ROI. The regression uses ordinary least squares, and the results are Fisher-transformed correlation coefficients between pairs of ROI.

Cluster-level inferences - Effective network connectivity

Second-level analyses of cluster-level inferences were calculated as follows. A general linear model analysis of individual subject connectivity matrices from the first-level anal-

X	Y	Z	Label	Brain Region(s)
24	-96	4	R_V1_V2_V3V	Right secondary visual
64	-41	21	R_STG_IPL	Right superior temporal gyrus, inferior parietal lobule
-55	-47	11	L_AngGyrus	Left angular gyrus
32	-43	-20	R_FusiForm	Right fusiform gyrus
33	-52	60	R_SPL_IPS_hIP3	Right superior parietal lobule, intraparietal sulcus, human intraparietal area 3
42	41	9	R_dlPFC	Right dorsolateral prefrontal cortex
-34	-1	44	L_PM_Mtr	Left premotor, motor
29	1	-1	R_Putamen	Right putamen
-39	49	10	L_dlPFC	Left dorsolateral prefrontal cortex
-22	-37	67	L_PrimSS_Mtr_SPL	Left primary somatosensory, motor, superior parietal lobule
52	-70	1	R_V5	Right visual
-46	-47	-21	L_FusiForm	Left fusiform
28	-45	52	R_PrimSS_SPL	Right primary somatosensory, superior parietal lobule
-58	-19	36	L_PrimSS_IPL	Left primary somatosensory, inferior parietal lobule
31	-30	-24	R_FusiForm	Right fusiform
-53	6	45	L_PM_BA44	Left premotor, Brodmann Area 44
-10	59	31	L_aPFC	Left anterior prefrontal cortex
55	-50	-28	R_ITG	Right inferior temporal gyrus
1	59	33	R_FP	Right frontal pole

Table 5.1: Peaks and sub-peaks of activity extracted from clusters obtained in Aim 2 results (see Table 4.2 on page 62)

ysis produced a matrix of F-values for both conditions of interest (hand or prosthesis). A hierarchical clustering procedure (Sørenson, 1948) was used to group ROI by functional similarity. These connection sets were then analyzed using both within- and between-network connectivity sets (Jafri et al., 2008), using a multivariate parametric general linear model for all connections, yielding an F-statistic (correlation measure) for each pair of networks, along with an uncorrected cluster-level p-value, and a false discovery rate-corrected p-value (Benjamini & Hochberg, 1995). The present analyses used an FDR-corrected $p < 0.05$ cluster-level threshold, and an uncorrected $p < 0.05$ connection-level threshold to select for connections with the largest effects to produce thresholded connectivity matrices.

Graph measures

Non-directional graphs with ROI represented as nodes, and above-threshold connections between nodes represented as edges were produced from adjacency matrices for each subject.

The adjacency matrices were calculated by thresholding the connectivity matrices at $z > 0.5$. These adjacency matrices were used to calculate additional graph-theoretical measures, of which clustering coefficient is considered here.

5.5 Results

To gain understanding related to changes in effective connectivity and graph-theoretic measures of cortical networks recruited when observing either a hand or prosthesis performing reach-to-grasp actions, we performed connectivity and graph-theoretic analyses of data previously collected during a BOLD activation and repetition suppression study (Chapter 4 on page 45). This allowed testing our hypothesis that watching the prosthesis perform reach-to-grasp tasks would result in decreased effective connectivity of brain areas comprising the action observation network compared to watching the hand perform the same tasks. We also tested our hypothesis that network properties would reflect more dispersed information flow in the prosthesis condition than in the intact condition.

5.5.1 Effective connectivity

While watching the hand reach-to-grasp

Network connectivity of clustered ROI developed while watching a hand reaching for objects are shown in Figure 5.2 on page 77 and their effect sizes in Table 5.2a on page 79. Connectivity analysis reveals four functionally-defined networks. The network shown in Figure 5.2a on page 77 shows classic connectivity from visual to dorsal and ventral streams (Goodale et al., 1994; Milner & Goodale, 2008; Goodale & Milner, 1992). The network in Figure 5.2d on page 77 shows connectivity characteristic of the action observation network (Kilner, Friston, & Frith, 2007). The network shown in Figure 5.2c on page 77 suggests information flow between these two networks.

While watching the prosthesis reach-to-grasp

Effective network connectivity of clustered ROI developed while watching a prosthesis reaching for objects are shown in Figure 5.3 on page 78 and their effect sizes in Table 5.2b on page 79. Connectivity analysis results in seven functionally-defined networks. Beginning with the network overview in Figure 5.3h on page 78, we see several small networks with little cohesive structure. For example, the network in Figure 5.3g on page 78 shows information flow between early visual areas and dorsal areas, and also to left angular gyrus. Similarly, in Figure 5.3f on page 78 we see connectivity from visual and inferior parietal lobule to dorsal and dorsolateral prefrontal cortex. Figure 5.3a on page 78 shows a ventral network with internal connectivity between primary sensory cortex, superior parietal lobule and inferior parietal lobule, while Figure 5.3b on page 78 shows a network between primary sensory and superior parietal lobule to left primary sensory and right visual superior temporal gyrus areas. Other small networks appear in right visual and superior temporal gyrus Figure 5.3c on page 78, prefrontal areas (Figure 5.3d on page 78), and premotor-motor areas (Figure 5.3e on page 78).

Hand

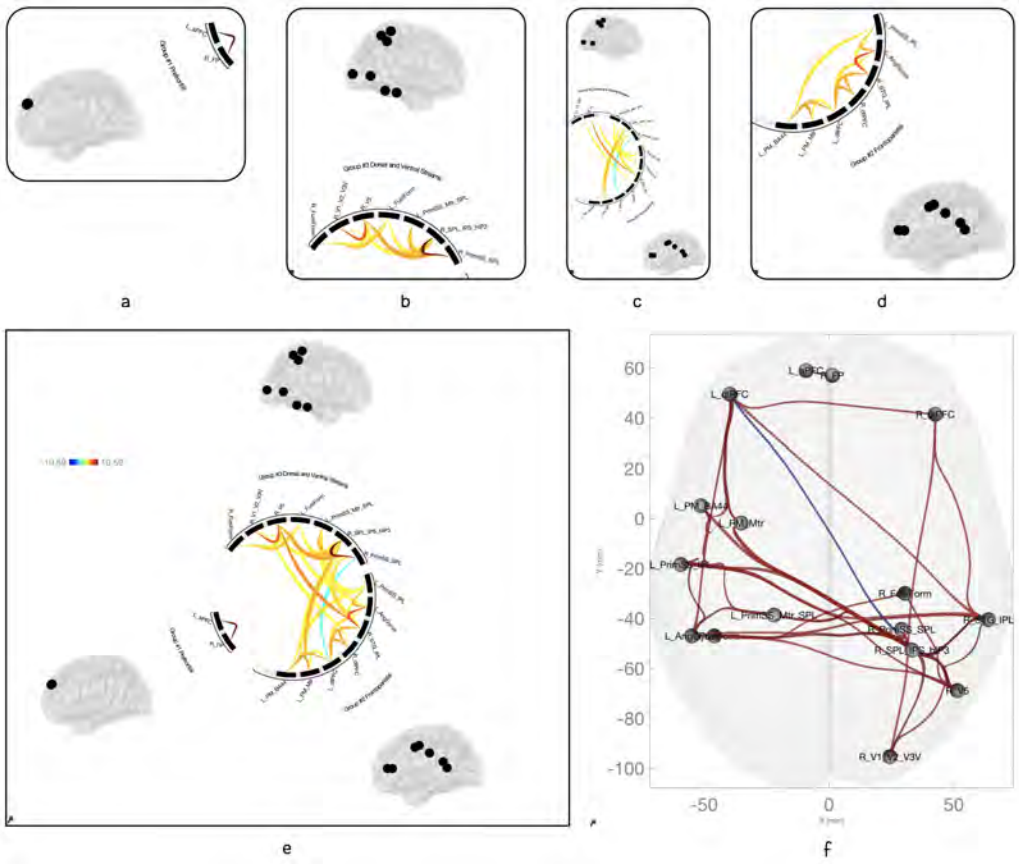

Figure 5.2: Effective network connectivity while watching a hand reach-to-grasp. In all figures warm colors indicates increased connectivity, while cool colors indicated decreased connectivity. Parametric multivariate statistics (Jafri et al., 2008). Cluster threshold: $p < 0.05$ cluster-level p-FDR corrected (MVPA omnibus test); connection threshold: $p < 0.05$ p-uncorrected. See Table 5.1 on page 74 for label descriptions. (a) Left anterior prefrontal cortex to right frontal pole (b) Primary and secondary visual areas to dorsal and ventral streams (c) Primary and secondary visual areas to supramarginal, frontoparietal and premotor areas (d) Network connectivity within supramarginal, frontoparietal and premotor areas (e) Connectome of all networks (f) Networks depicted on a glass brain.

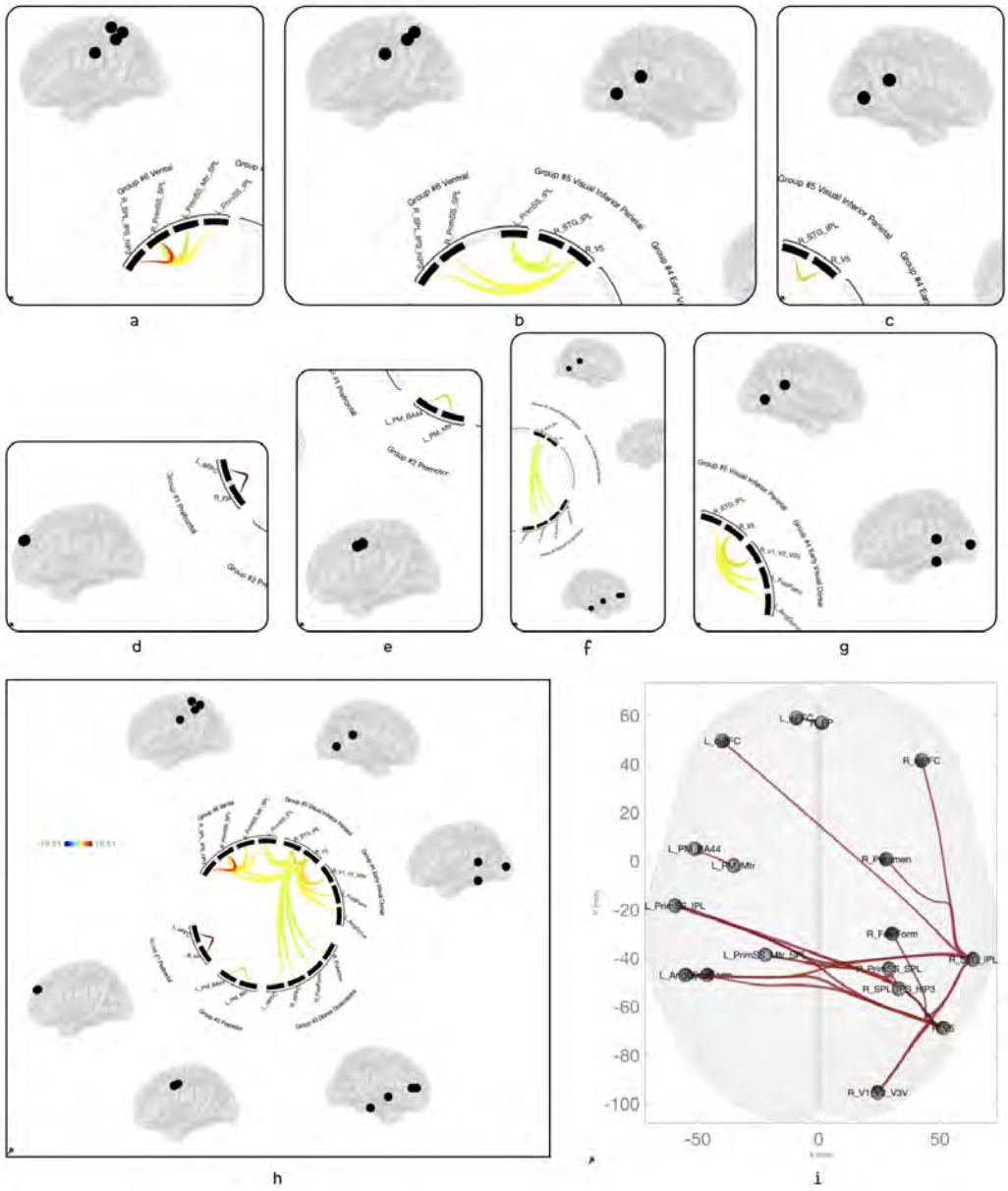

Figure 5.3: Effective network connectivity while watching a prosthesis reach-to-grasp. In all figures warm colors indicates increased connectivity, while cool colors indicated decreased connectivity. See Table 5.1 on page 74 for label descriptions. (a) Primary motor, primary somatosensory to superior parietal lobule and inferior parietal lobule (b) Right visual, superior temporal gyrus, inferior parietal lobule to right primary sensory, superior parietal lobule, intraparietal sulcus, hIP3 (c) Right visual, superior temporal/supramarginal gyrus, inferior parietal lobule (d) Left anterior prefrontal cortex to right frontal pole (e) Left primary motor, premotor, Brodmann Area 44 (f) Right visual, superior temporal gyrus, inferior parietal lobule to right putamen, fusiform, dorsolateral prefrontal cortex, left dorsolateral prefrontal cortex (g) Right visual, superior temporal gyrus, inferior parietal lobule to right early visual areas, left fusiform, left angular gyrus (h) Connectome of all networks (i) Networks depicted on a glass brain.

Hand

Network	F(1,14)	p-unc	p-FDR	Effect Size
a	122.23	<0.001	<0.001	0.527
b	97.41	<0.001	<0.001	0.187
c	8.88	0.010	0.022	0.111
d	58.19	<0.001	<0.001	0.167

(a) F-values for networks in Figure 5.2.

Prosthesis

Cluster	F(1,14)	p-unc	p-FDR	Effect Size
a	116.21	<0.001	<0.001	0.233
b	17.33	<0.001	0.004	0.169
c	41.67	<0.001	<0.001	0.225
d	215.11	<0.001	<0.001	0.540
e	39.02	<0.001	<0.001	0.279
f	11.59	0.004	0.016	0.136
g	70.93	<0.001	<0.001	0.215

(b) F-values for networks in Figure 5.3.

Table 5.2: Statistical measures of the networks presented in the indicated networks. Parametric multivariate statistics (cluster-level inferences, Effective Network Connectivity, (Jafri et al., 2008)) cluster threshold: $p < 0.05$ cluster-level p-FDR corrected (MVPA omnibus test); connection threshold: $p < 0.05$ p-uncorrected.

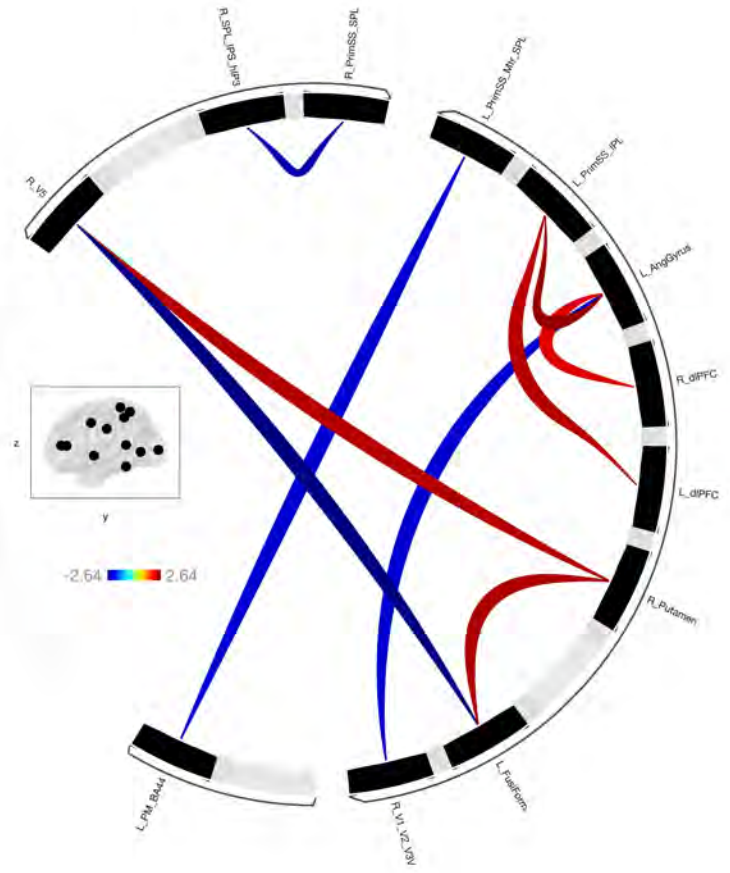

Figure 5.4: Effective connectivity differences between watching a hand and a prosthesis. Red = Hand > Prosthesis, Blue = Prosthesis > Hand. The colorbar represents T values. Please see Table 5.3 on the next page for statistics. Clustering threshold $p < 0.05$ uncorrected, connection threshold $p < 0.05$ uncorrected.

Condition	Connection		Statistic	p-unc	p-FDR
Hand > Prosthesis					
	L_PrimSS_IPL	L_AngGyrus	T(14) = 2.52	0.025	0.843
	R_Putamen	L_FusiForm	T(14) = 2.38	0.032	0.843
	R_V5	R_Putamen	T(14) = 2.38	0.032	0.843
	L_PrimSS_IPL	L_dlPFC	T(14) = 2.36	0.033	0.843
	L_dlPFC	L_PrimSS_IPL	T(14) = 2.24	0.042	0.843
	R_dlPFC	L_AngGyrus	T(14) = 2.15	0.049	0.843
Prosthesis > Hand					
	L_FusiForm	R_V5	T(14) = -2.64	0.019	0.843
	R_PrimSS_SPL	R_SPL_IPS_hIP3	T(14) = -2.39	0.032	0.843
	R_V1_V2_V3V	L_AngGyrus	T(14) = -2.24	0.042	0.843
	L_PM_BA44	L_PrimSS_Mtr_SPL	T(14) = -2.23	0.042	0.843

Table 5.3: Statistics for connectivity differences shown in Figure 5.4 on the previous page. Positive T values are red in the figure, negative are blue. Clustering threshold $p < 0.05$ uncorrected, connection threshold $p < 0.05$ uncorrected.

5.5.2 Network-theoretic measures

Graph theory - Clustering coefficient

Network theoretic analyses were performed for participants watching either a hand or prosthesis reaching for objects. The resulting graphs of networks and clustering coefficient are shown in Figure 5.5 on the following page with statistical measures presented in Table 5.4 on the next page. The clustering coefficient measures the proportion of connected edges within the local subgraph for each node, and is a measure of local integration. The clustering coefficient for the left angular gyrus node (L_AngGyrus) was statistically significantly greater in the hand condition than the prosthesis condition ($\text{beta} = 0.24, T(1, 14) = 4.39, p_{unc} = 0.002, p_{FDR} = 0.035$). The clustering coefficient of the left premotor/motor node is not statistically significant in the prosthesis condition. Differences in clustering coefficient between conditions in left primary sensory/inferior parietal lobule, bilateral dorsolateral prefrontal cortex, right superior parietal lobule/intraparietal sulcus/hIP3, and right early visual areas (V1, V2, V3V), reveal important differences in network properties, although these differences lack statistical significance.

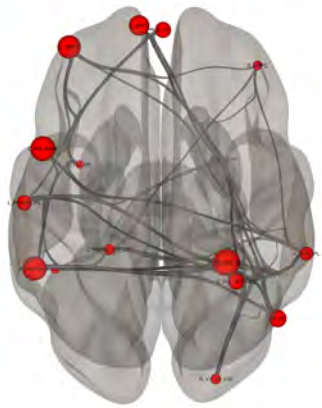

(a) Networks while watching the hand reach for objects.

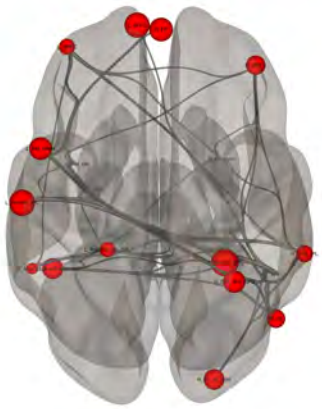

(b) Networks while watching the prosthesis reach for objects.

Figure 5.5: Network graphs with sphere diameter proportional to clustering coefficient beta values.

	Hand (Figure 5.5a)					Prosthesis (Figure 5.5b)				
ROI	beta	T	dof	p-unc	p-FDR	beta	T	dof	p-unc	p-FDR
network	0.32	13.02	14	<0.001		0.30	10.96	14	0.000	
L_AngGyrus	0.35	7.50	12	<0.001	<0.001	0.17	3.75	9	0.005	0.007
L_aPFC	0.35	6.33	11	<0.001	<0.001	0.37	3.58	12	0.004	0.006
L_dlPFC	0.32	7.20	13	<0.001	<0.001	0.24	3.22	10	0.009	0.011
L_FusiForm	0.29	3.09	6	<0.021	0.024	0.31	3.27	6	0.017	0.020
L_PM_BA44	0.37	7.74	10	<0.001	<0.001	0.34	3.63	11	0.004	0.006
L_PM_Mtr	0.38	2.54	7	<0.031	0.041				n.s.	
L_PrimSS_IPL	0.30	4.65	12	<0.001	<0.001	0.38	5.60	13	<0.001	<0.001
L_PrimSS_Mtr_SPL	0.30	3.32	11	0.007	0.010	0.23	3.92	11	0.002	0.005
R_dlPFC	0.21	2.96	7	0.021	0.024	0.29	3.32	11	0.007	0.010
R_FP	0.37	4.97	12	<0.001	<0.001	0.35	4.93	12	<0.001	<0.001
R_PrimSS_SPL	0.31	8.43	13	<0.001	<0.001	0.41	5.56	14	<0.001	0.001
R_SPL_IPS_hIP3	0.30	5.06	14	<0.001	<0.001	0.33	5.15	14	<0.001	<0.001
R_STG_IPL	0.28	4.31	13	<0.001	0.001	0.25	5.91	14	<0.001	<0.001
R_V1_V2_V3V	0.42	3.21	7	0.014	0.020	0.31	4.40	11	0.001	0.002
R_V5	0.29	5.43	14	<0.001	<0.001	0.27	7.24	13	<0.001	<0.001

Table 5.4: Clustering coefficient statistics for the indicated networks. Degrees of freedom (dof) for each node reflects the number of participants for which the ROI connectivity exceeded threshold. ROI absent connectivity for individual participants were omitted from statistical calculations.

5.6 Discussion

The present study sought to evaluate cognitive differences when watching either a hand or an unfamiliar end-effector perform reach-to-grasp tasks. More specifically, we sought to compare differences in effective connectivity between brain regions previously determined to be active while observing these actions. We also sought to compare differences in the network-theoretic property of clustering coefficient during the same observations. Our findings reveal end-effector modulated differences in network formation, effective connectivity, and clustering coefficient.

We hypothesized that watching the prosthesis perform reach-to-grasp tasks would result in decreased effective connectivity of brain areas comprising the action observation network compared to watching the hand perform the same tasks. Our findings support our hypothesis. While watching the hand reach to grasp, there was increased effective connectivity between visual, parietal, and dorsolateral prefrontal regions. Additionally, while watching the prosthesis, connectivity to left premotor/motor areas did not reach significance.

We also hypothesized that network properties would reflect more global, rather than local, information flow in the prosthesis condition than in the intact condition. Findings do not support this hypothesis, though statistical power did not reach threshold except in the left angular gyrus. Compared to watching a hand carry out the reach-to-grasp actions, when watching the prosthesis we see higher clustering coefficient in left angular gyrus, right dorsolateral prefrontal cortex, early visual, prefrontal, and right superior parietal lobule/intraparietal sulcus.

5.6.1 Watching the prosthesis reach-to-grasp does not fully engage the action observation network

There are many studies investigating brain activity and commonalities between actions that we execute, and actions that we observe. When participants watched either the hand or

prosthesis reach to grasp objects, the intention of the actions had been provided by the prompt text (e.g. "Drink the coffee"). This priming and observation of the hand resulted in development of effective connectivity of cortical areas associated with the action observation network, while the action observation network was not fully recruited while watching the prosthesis. In fact, effective connectivity became lower in clusters associated with the left angular gyrus and left primary somatosensory/inferior parietal lobule, and bilateral dorsolateral prefrontal cortex. Reduced connectivity was also seen between visual V5 and right putamen, and between right putamen and left fusiform clusters.

This suggests the participants' lack of experience with the prosthesis translates to a lack of visual-motor associations as previously described. This led to failure to fully recruit the complete action observation network and its generative and predictive systems. As discussed in the introduction, this system is not only a "kinematics in, intention out" network as was previously thought (Rizzolatti & Craighero, 2004), but also incorporates reciprocal feedback from higher to lower levels to update probabilities at each level of the system (Kilner, Friston, & Frith, 2007).

5.7 Conclusions

The current study sought to examine how connectivity between brain regions differs when observing a prosthesis performing reach-to-grasp actions or a hand performing the same actions. Watching the hand resulted in greater and more highly clustered effective connectivity between brain regions known to form the action observation network. Watching the prosthesis resulted in the formation of more fragmented clusters with fewer inter-cluster connections. Failure to form effective connectivity between regions associated with the action observation network suggests the lack of a sensorimotor mapping between the observed kinematics of the prosthesis and the motor commands that would create those kinematics. This lack of information for which the action observation network is specialized results in different connectivity patterns that reflect different cognitive processes for determining

the intention of actions carried out with the prosthesis. In turn, this differing cognitive processing may be a contributing factor in prosthesis abandonment. Programs to develop the sensorimotor relationships of prothesis use may improve outcomes of training and rehabilitation programs for acute and chronic prosthesis users.